AMERICAN SOCIETY FOR MICROBIOLOGY | Journal of Virology®

VIRUS-CELL INTERACTIONS

Evidence for Viral mRNA Export from Ebola Virus Inclusion Bodies by the Nuclear RNA Export Factor NXF1

Lisa Wendt,[a] Janine Brandt,[a] Dmitry S. Ushakov,[a] Bianca S. Bodmer,[a] Matthew J. Pickin,[b] Allison Groseth,[a] Thomas Hoenen[a]

[a]Institute of Molecular Virology and Cell Biology, Friedrich-Loeffler-Institut, Greifswald-Insel Riems, Germany
[b]Institute of Novel and Emerging Infectious Diseases, Friedrich-Loeffler-Institut, Greifswald-Insel Riems, Germany

ABSTRACT Many negative-sense RNA viruses, including the highly pathogenic Ebola virus (EBOV), use cytoplasmic inclusion bodies (IBs) for viral RNA synthesis. However, it remains unclear how viral mRNAs are exported from these IBs for subsequent translation. We recently demonstrated that the nuclear RNA export factor 1 (NXF1) is involved in a late step in viral protein expression, i.e., downstream of viral mRNA transcription, and proposed it to be involved in this mRNA export process. We now provide further evidence for this function by showing that NXF1 is not required for translation of viral mRNAs, thus pinpointing its function to a step between mRNA transcription and translation. We further show that RNA binding of both NXF1 and EBOV NP is necessary for export of NXF1 from IBs, supporting a model in which NP hands viral mRNA over to NXF1 for export. Mapping of NP-NXF1 interactions allowed refinement of this model, revealing two separate interaction sites, one of them directly involving the RNA binding cleft of NP, even though these interactions are RNA-independent. Immuno-fluorescence analyses demonstrated that individual NXF1 domains are sufficient for its recruitment into IBs, and complementation assays helped to define NXF1 domains important for its function in the EBOV life cycle. Finally, we show that NXF1 is also required for protein expression of other viruses that replicate in cytoplasmic IBs, including Lloviu and Junín virus. These data suggest a role for NXF1 in viral mRNA export from IBs for various viruses, making it a potential target for broadly active antivirals.

IMPORTANCE Filoviruses such as the Ebola virus (EBOV) cause severe hemorrhagic fevers with high case fatality rates and limited treatment options. The identification of virus-host cell interactions shared among several viruses would represent promising targets for the development of broadly active antivirals. In this study, we reveal the mechanistic details of how EBOV usurps the nuclear RNA export factor 1 (NXF1) to export viral mRNAs from viral inclusion bodies (IBs). We further show that NXF1 is not only required for the EBOV life cycle but also necessary for other viruses known to replicate in cytoplasmic IBs, including the filovirus Lloviu virus and the highly pathogenic arenavirus Junín virus. This suggests NXF1 as a promising target for the development of broadly active antivirals.

KEYWORDS Ebola virus, Junin virus, Lloviu virus, NXF1, filovirus, inclusion body, mRNA export, replication factory

Ebola virus (EBOV) is the causative agent of devastating outbreaks of severe hemorrhagic fever in West and Central Africa (1). Although recent progress has led to the approval of vaccines and therapeutic monoclonal antibodies (2, 3), EBOV infection remains a challenge in areas of endemicity. Antiviral drugs that are inexpensive and easy to administer would benefit the fight against this virus, as well as other filoviruses, enormously. Virus-host interactions, especially those that are conserved among several viruses known to occur in the same geographical regions, are promising targets for these types of antiviral drugs.

Editor Rebecca Ellis Dutch, University of Kentucky College of Medicine

Address correspondence to Thomas Hoenen, thomas.hoenen@fli.de.

The authors declare no conflict of interest.

Received 10 June 2022
Accepted 14 August 2022
Published 30 August 2022

However, many virus-host interactions that contribute to essential steps in the virus life cycle remain either poorly characterized or are completely unknown. For example, there is only limited knowledge of host cell factors supporting EBOV RNA synthesis and protein expression. On the viral side, EBOV RNA synthesis is driven by the viral nucleoprotein (NP), the viral polymerase (L), the polymerase cofactor viral protein 35 (VP35), and the transcriptional activator VP30, which together comprise the ribonucleoprotein (RNP) complex proteins (4, 5). However, EBOV also depends on the host cell to facilitate viral RNA synthesis and protein expression, not only for supplying nucleotides and the translation of viral mRNAs but also for the biological activity of specific host cell proteins. For example, kinases and phosphatases have been shown to modulate the activity of VP30 and thereby regulate viral transcription and replication (6–8). Further, other host cell factors, such as RBBP6, SMYD3, and hnRNP L, have been demonstrated to influence viral RNA synthesis (9–11).

EBOV RNA synthesis occurs in cytoplasmic inclusion bodies (IBs) (12, 13), the formation of which can be recapitulated by the expression of viral RNPs or even just by expression of the NP alone (14–16). For a growing number of negative-sense RNA viruses, IBs have been described as having properties of liquid organelles (17, 18), and EBOV IBs also appear to show some characteristic features of liquid organelles, although definitive proof for this is still lacking (12). Liquid organelles are formed by liquid-liquid phase separation, and their main constituents are often RNA and RNA-binding proteins, thus creating a favorable environment for RNA-related processes (for a review, see reference 19). However, nothing is known about how EBOV RNA species leave this environment and, in particular, how mRNAs are exported from IBs toward host ribosomes for translation.

Our previous work has suggested that the host cell factor nuclear RNA export factor 1 (NXF1) plays a role in facilitating this export (20). In uninfected cells, NXF1 is the key component of the mRNA export machinery responsible for driving the export of cellular mRNAs from the nucleus to the cytoplasm (for reviews, see references 21 and 22). However, this process involves many different proteins that hand over the cellular mRNA from one export adapter to the next, ensuring that only fully matured mRNAs leave the nucleus. One of the mechanisms involved in this handover is the conformational activation of NXF1 (23). NXF1 is a weak RNA-binding protein in its closed conformation, in which the RNA-binding domain (RBD) and the NTF2-like (NTF2) domain of NXF1 form an intramolecular interaction. Only upon interaction with two members of the transcription and export (TREX) complex, Aly and THOC5, which disrupt the intramolecular interaction between the RBD and the NTF2 domains, does NXF1 become able to strongly bind and subsequently export mRNAs from the nucleus. Many viruses with nuclear stages in their replication cycles hijack the nuclear mRNA export pathway by interacting with NXF1 or with export adapters such as Aly or Uif to promote the nuclear export of viral RNAs (24–27).

Although EBOV is not known to have a nuclear stage in its life cycle, our previous data suggest that NXF1 is usurped by EBOV to facilitate a late step in viral protein expression (20, 28). However, the precise step affected remained unclear. Further, while we could demonstrate that NXF1 interacts with both EBOV NP and EBOV mRNA (20), the details of this interaction and how EBOV recruits NXF1 into IBs also remained elusive. Here, we now further analyze the role of NXF1 and its individual domains in viral protein expression and demonstrate that NXF1 indeed facilitates mRNA export from IBs. Further, we identify mechanistic details of how interaction between NXF1 and EBOV NP mediates this function.

RESULTS

NXF1 interacts with authentic EBOV mRNA. For its proposed function in the EBOV life cycle, NXF1 must interact with viral mRNA species, and our previous study showed that NXF1 can interact with EBOV minigenome-derived mRNAs (20). However, the mRNA in this study did not encode a viral protein and was therefore only a surrogate for EBOV mRNAs. To confirm these results with authentic EBOV mRNA species, we performed coimmunoprecipitation (coIP) assays with NXF1 and NXF1 lacking its RNA-binding domain (NXF1-ΔRBD)

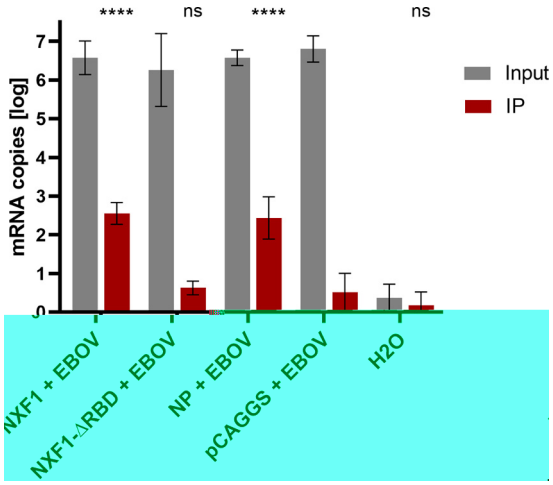

FIG 1 NXF1 interacts with authentic EBOV mRNAs. 293T cells were infected with rgEBOV and transfected with plasmids encoding flag/HA-tagged NXF1 or NP. Two days postinfection, cells were lysed, and flag-tagged proteins were precipitated using anti-flag antibodies. Coprecipitated RNA was isolated from the samples, and VP40-mRNA was quantified by RT-qPCR. Shown are the results of four independent experiments. Asterisks indicate *P* values from one-way ANOVA for the differences compared to pCAGGS + EBOV (ns, $P > 0.05$; **, $P \leq 0.01$; ***, $P \leq 0.001$; ****, $P \leq 0.0001$) for the IP samples.

in EBOV-infected cells and quantified the amount of coprecipitated VP40-mRNA (Fig. 1). Using this approach, we could show that VP40-mRNA was efficiently coprecipitated with NXF1, confirming the data previously obtained with EBOV minigenomic mRNA. Furthermore, NXF1-ΔRBD no longer coprecipitated VP40-mRNA, confirming that the RBD of NXF1 mediates the interaction with viral mRNAs. In addition, while there was so far no evidence showing binding of viral mRNAs (or the lack thereof) by NP, this experiment also revealed that EBOV NP interacts with viral mRNA, a possibility that had previously been dismissed by some in the field.

NXF1 is not required for translation of viral mRNAs. We have previously shown that NXF1 is important for a late step in EBOV protein expression, as indicated by small interfering RNA (siRNA)-mediated knockdown of NXF1, which resulted in reduced viral protein expression but did not affect viral mRNA synthesis (20). To further narrow down the role of NXF1 in EBOV protein expression, we assessed the importance of NXF1 for the translation of EBOV mRNAs. To this end, we transfected cells in which NXF1 had been knocked down by siRNAs with *in vitro* transcribed EBOV minigenome mRNAs encoding nanoluciferase and analyzed the resulting reporter activity (Fig. 2A). We observed comparable reporter activity in cells treated with anti-NXF1 siRNA and in control cells, indicating that depletion of NXF1 has no impact on the translation of EBOV mRNAs. To ensure efficient siRNA-mediated knockdown of NXF1 was taking place, we performed EBOV minigenome assays in parallel, and, here, siRNA-mediated knockdown of NXF1 led to a strong decrease in reporter activity of 0.8 $\log_{10}$ or 83% (Fig. 2B), consistent with our previous report (20).

NXF1-RBD and NXF1-NTF2 are sufficient for interaction with NP. We demonstrated previously that the RBD of NXF1 is sufficient to mediate interaction with EBOV NP in a manner that was not dependent on the presence of RNA, but rather was weakened by RNA binding of NXF1, whereas the RNA recognition motif (RRM) was unable to do so (20). However, it remained unclear whether the other three domains of NXF1—the leucine-rich repeat (LRR) domain, the NTF2 domain, and the ubiquitin-associated (UBA) domain—can also interact with NP. To investigate this, we performed coIP assays with these domains and EBOV NP (Fig. 3). To exclude RNA-dependent interactions, coIPs were performed in the presence of RNase A. In the case of the LRR domain, a construct expressing both the RRM and the LRR domain (RRM-LRR) was used, since it was not possible to precipitate the LRR domain when it was expressed alone. This construct did not coprecipitate NP, indicating that the LRR domain is not sufficient to mediate interaction with NP. In contrast,

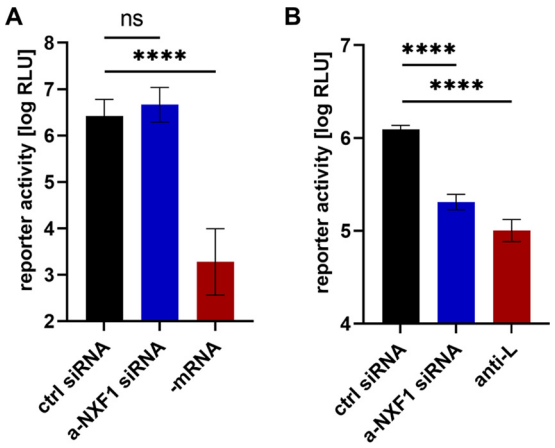

FIG 2 NXF1 is not important for the translation of viral mRNAs. (A) Influence of siRNA-mediated knockdown of NXF1 on viral translation. 293T cells were reverse transfected with siRNAs targeting NXF1 or a negative-control (ctrl) siRNA. At 2 days posttransfection, cells were transfected with firefly mRNA and nanoluciferase encoding EBOV minigenome mRNA. As a control, the EBOV mRNA was omitted (–mRNA). Another 2 days later, cells were harvested and reporter activity was measured. Nanoluciferase reporter activity was normalized to firefly reporter activity. (B) Influence of siRNA-mediated knockdown of NXF1 on viral RNA synthesis and protein expression. 293T cells were transfected with siRNAs targeting NXF1, EBOV L, or a negative control siRNA. At 2 days posttransfection, cells were transfected with plasmids encoding the classical EBOV minigenome (pT7-EBOV-1cis-vRNA-hrluc), as well as plasmids encoding T7, EBOV L, NP, VP30, VP35, and firefly luciferase as a control. Another 2 days later, cells were harvested, reporter activity was determined and *Renilla* luciferase activity was normalized to firefly activity. Shown are the means and standard deviations of four independent experiments. Asterisks indicate *P* values from one-way ANOVA (ns, $P > 0.05$; ****, $P \leq 0.0001$).

precipitation of the NTF2 domain resulted in coprecipitation of EBOV NP, showing that this domain is sufficient for interaction with NP. Finally, while we were able to express the NXF1-UBA domain alone, we were not able to precipitate this domain, so no conclusion can be drawn regarding its ability to interact with NP.

NXF1-NTF2 and NXF1-UBA domains are recruited into NP-derived IBs. Next, we assessed the intracellular localization of individual NXF1 domains and particularly their recruitment into NP-induced IBs (Fig. 4), which EBOV NP is known to be able to form when expressed alone (16). Expression of the RBD showed a nuclear localization, while the RRM domain could mainly be detected in speckles predominantly found in the cytoplasm (Fig. 4A). In contrast, the LRR, NTF2, and UBA domains localized diffusely both in the cytoplasm and in the nucleus. The nuclear localization of the RBD remained unchanged upon coexpression with NP, suggesting that the RBD alone is not recruited into NP-derived IBs (Fig. 4B and C). Coexpression of the RRM or LRR domain with NP led to a similar observation, since these domains did not colocalize with NP-derived IBs either. In contrast, both the NTF2 and the UBA domains showed a colocalization with NP, indicating that either of these two domains is sufficient for recruitment of NXF1 into IBs. This suggests that the interaction of the RBD domain of NXF1 with NP, as observed by coIP in cell lysates, does not contribute to relocalization of NXF1 into IBs but rather that a relocalization to IBs is facilitated by these other domains as a prerequisite for NP interaction with the RBD to take place.

NXF1-RRM is dispensable for the function of NXF1 in the EBOV life cycle. After having assessed the individual domains of NXF1 for their interaction with EBOV NP and for recruitment into IBs, we next assessed their functional relevance for EBOV protein expression. To this end, we performed EBOV minigenome assays in cells in which NXF1 had been knocked down and cotransfected either wild-type NXF1, different NXF1 deletion mutants, or single domains of NXF1, all of which contained silent mutations in the siRNA binding site (here called ΔsiRNA), or in the case of NXF1 constructs without the RRM domain lacked the siRNA binding site completely (Fig. 5A). To ensure that the observed effects were not caused by differences in expression levels of the different NXF1 variants, the amounts of transfected plasmid were adjusted for each construct individually to ensure comparable

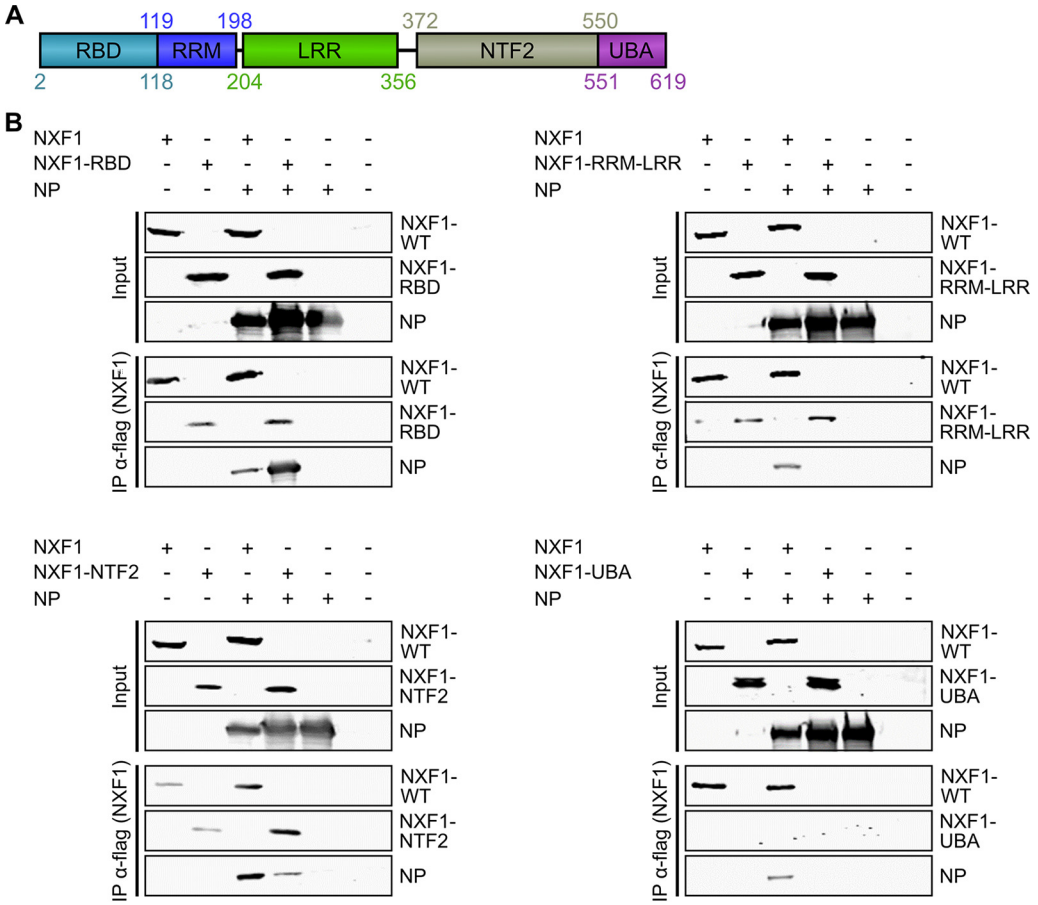

FIG 3 NXF1-RBD and NXF1-NTF2 are sufficient for interaction with EBOV NP. (A) Structural organization of NXF1. Numbers indicate amino acid positions. (B) Coimmunoprecipitation of NXF1 domains and EBOV NP. 293T cells were transfected with plasmids encoding flag/HA-tagged NXF1 or the different NXF1 domains, as well as the plasmid for myc-tagged EBOV NP, as indicated. At 2 days posttransfection, NXF1 or NXF1 domains were precipitated with anti-flag antibodies, and input and precipitates were subsequently analyzed via SDS-PAGE and Western blotting. NXF1 and NP were detected with antibodies specific for the HA and myc tags, respectively. Representative results from four independent experiments are shown.

expression levels, and these levels were assessed via Western blotting for each experiment, with reporter activity values being included in further analysis only if the expression level was in the range of 50 to 200% of wild-type NXF1-ΔsiRNA. Using this approach, we could show that siRNA-mediated knockdown can be complemented by transfecting wild-type NXF1-ΔsiRNA. The same effect was observed with the NXF1-ΔRRM construct. In contrast, the NXF1 constructs lacking any of the other four domains of NXF1 failed to rescue the siRNA-mediated knockdown of NXF1, and the same could also be observed for a construct consisting of only the RBD and the NTF2 domain (RBD-NTF2). A ΔRRM-ΔLRR construct, which only lacked domains not important for interaction with NP (Fig. 3) or for localization in IBs (Fig. 4B and C), also failed to rescue reporter activity. This suggests that all NXF1 domains, except the RRM, are required to facilitate the function of NXF1 in the EBOV life cycle and that this is not exclusively dictated by their interaction with NP and associated recruitment to IBs.

To further control for the possibility that the deletion of parts of NXF1 could lead to an altered intracellular localization that might influence the availability of NXF1 for recruitment into EBOV IBs, we performed immunofluorescence analyses with the NXF1 mutants used in the complementation assay (Fig. 5B). All constructs showed similar localization patterns, which are also comparable with WT NXF1, and, importantly, they could be found both in the cytoplasm and in the nucleus.

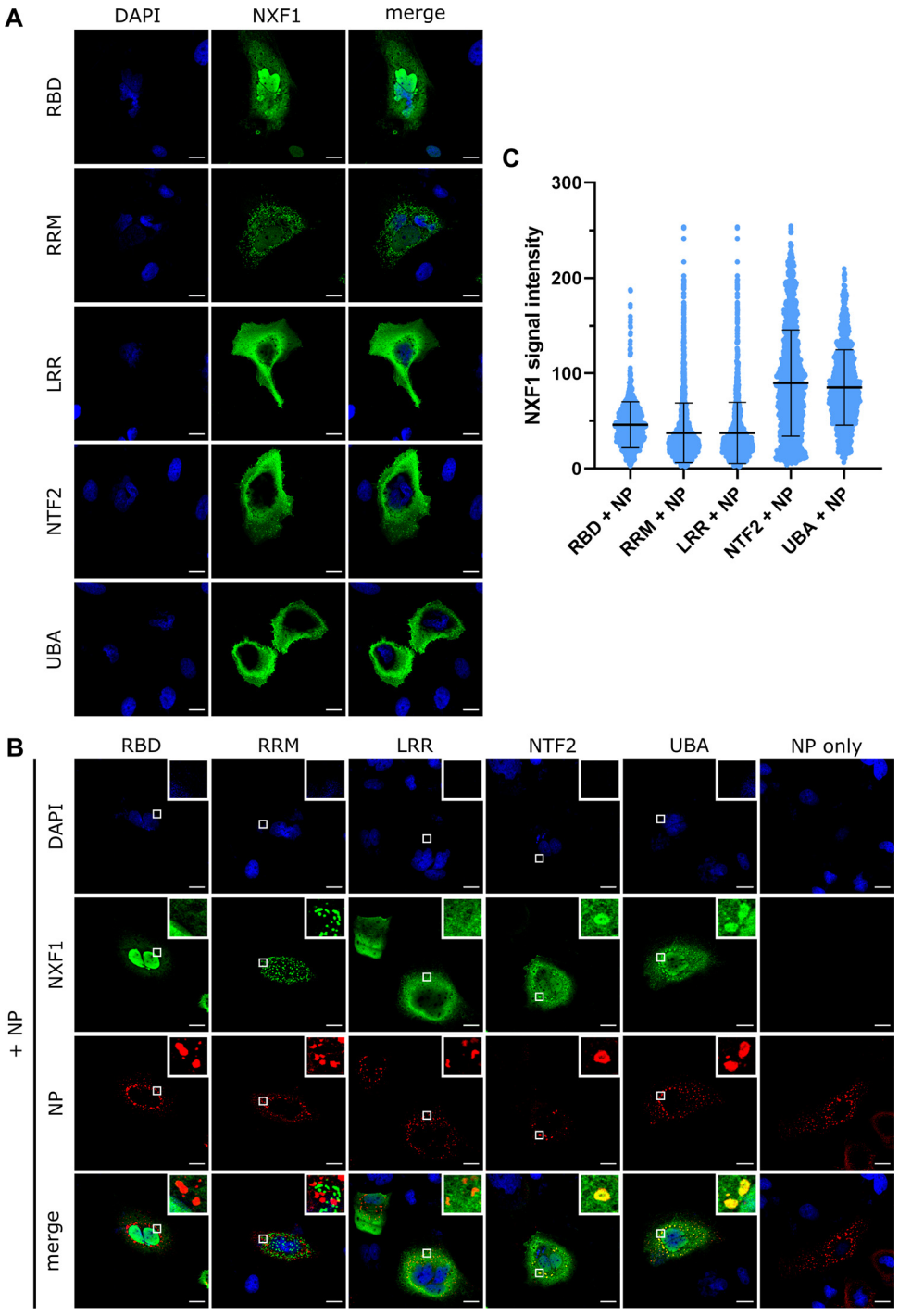

FIG 4 Localization studies using NXF1 domains show that NXF1-NTF2 and NXF1-UBA are sufficient for recruitment into NP-derived IBs. (A) Immunofluorescence analysis of NXF1 domains. Huh7 cells were transfected with expression plasmids for the different flag/HA-tagged NXF1 domains. At 2 days posttransfection, cells were fixed with 4% paraformaldehyde and permeabilized. For the detection of NXF1 domains (shown in green), anti-flag antibodies were used, and nuclei (shown in blue) were stained with DAPI. (B) Coimmunofluorescence analysis. Huh7 cells overexpressing the different flag/HA-tagged NXF1 domains and EBOV NP were fixed at 48 h posttransfection. After permeabilization of the cells, flag/HA-NXF1 domains (shown in green) were detected with anti-flag antibodies; for the detection of NP-myc (shown in red), an anti-myc antibody was used. Staining of nuclei (shown in blue) was achieved by using DAPI, and cells were visualized by confocal laser scanning microscopy. Scale bars indicate 20 μm, and insets show magnifications of the indicated areas. (C) Quantification results. Mean fluorescence intensity of NXF1 in IBs was determined using Arivis Vision 4D software. Shown are all values for IBs with a surface area of $>$0.2 μm^2.

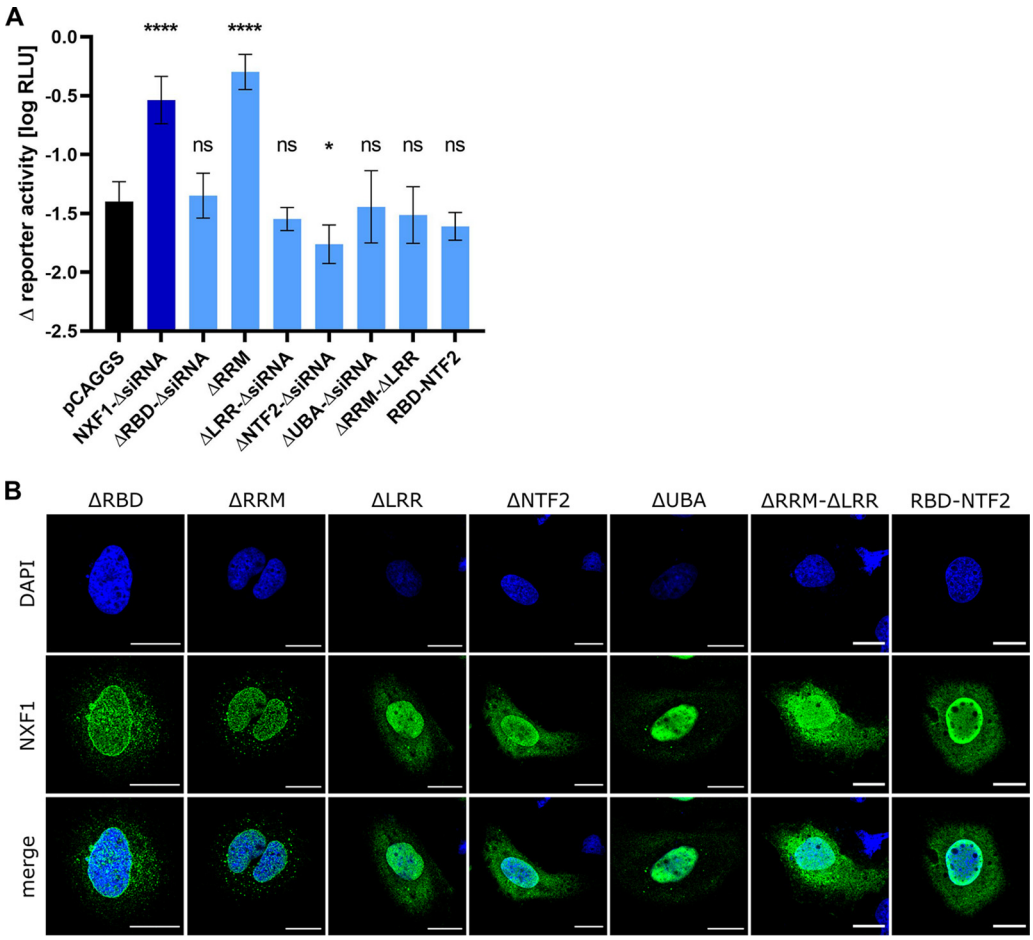

FIG 5 Contribution of different NXF1 domains to the function of NXF1 in the EBOV life cycle. (A) Complementation assay. 293T cells were reverse transfected with siRNAs targeting NXF1. At 48 h posttransfection, cells were transfected with all EBOV minigenome components, as well as the indicated NXF1 constructs or empty vector (pCAGGS) as a control. At 2 days after the minigenome transfection, cells were harvested, and the reporter activity was measured. Minigenome reporter activity was normalized to firefly activity. Shown are the means and standard deviations for at least three independent experiments. Asterisks indicate *P* values from one-way ANOVA (ns, $P > 0.05$; *, $P \leq 0.05$; ****, $P \leq 0.0001$). (B) Immunofluorescence analysis of different NXF1 constructs. Huh7 cells were transfected with the expression plasmids for the different flag/HA-tagged NXF1 constructs. At 2 days posttransfection, cells were fixed with 4% paraformaldehyde, permeabilized, and stained with anti-flag antibodies (green) for the detection of NXF1 and DAPI (blue) for the detection of nuclei. Scale bars, 20 μm.

Interaction with NXF1 is mediated by the core fragment of NP. While the interaction sites for EBOV NP within NXF1 could be pinpointed to the RBD and the NTF2 domains of NXF1, the region of NP that is necessary for the interaction with these two NXF1 domains remained unknown. EBOV NP can be divided into an amino-terminal domain (NTD) containing the central NP core fragment, which mediates RNA binding by NP and NP:NP interactions, as well as a carboxy-terminal domain (CTD), which is necessary for the formation of IBs and the incorporation of nucleocapsids into viral particles (Fig. 6A) (15, 29–32). In order to identify the region of NP involved in binding of NXF1, we first performed coIPs between the NXF1-RBD or the NTF2 domain and the amino-terminal portion of NP in the presence of RNase A (Fig. 6B). These coIPs revealed that both the RBD and the NTF2 domain interact with the NP-NTD and that they rely on the core fragment within the NTD for this interaction. In fact, the interaction between both NXF1 domains and the NP core appears to be stronger than the interaction with the whole NTD, possibly due to influences of NP regions outside the core on core structure or accessibility. In contrast, the C-terminal tail (C-tail) was not required for the interaction of NP with either of the two NXF1 domains, although the interaction

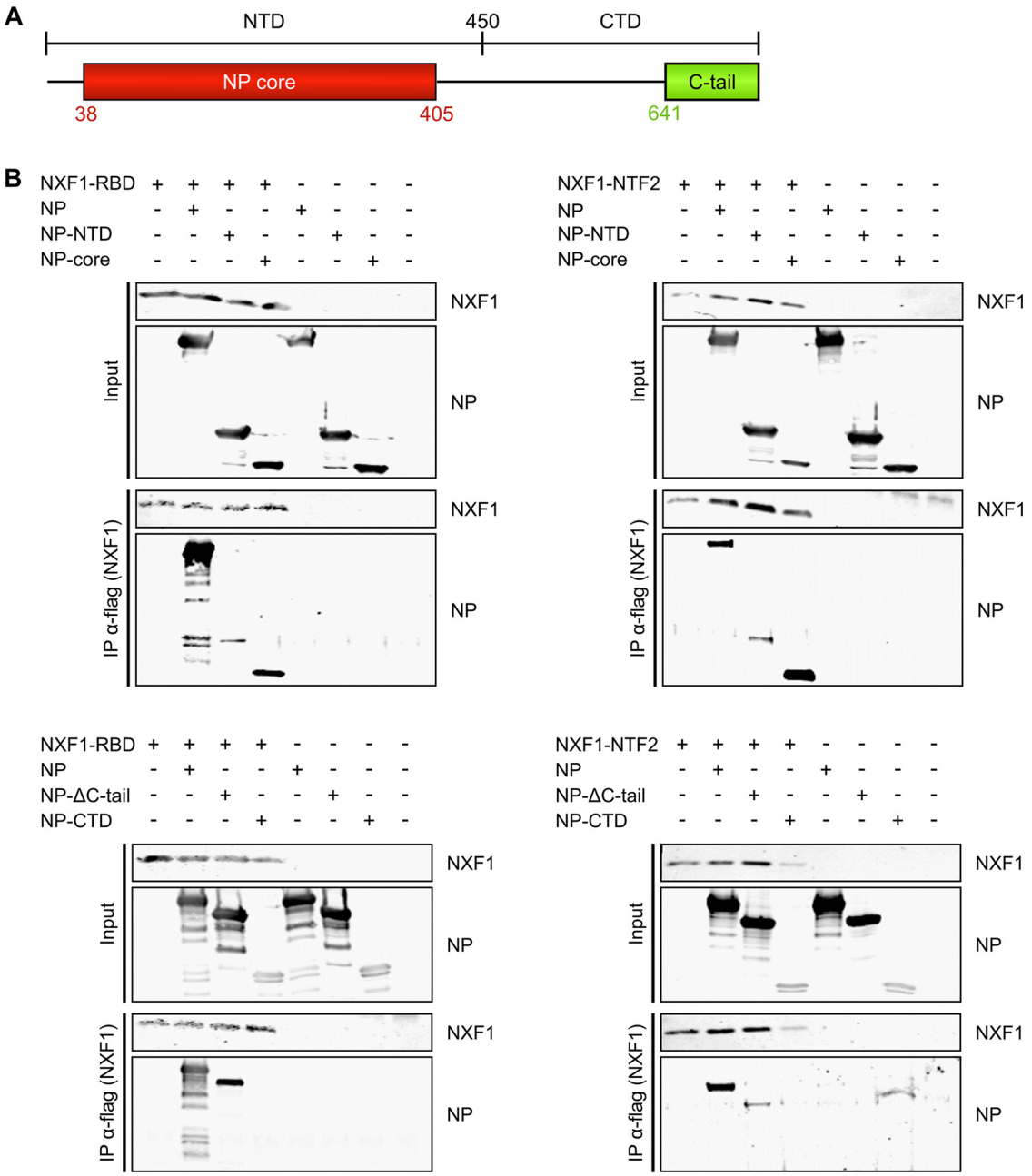

FIG 6 NXF1-RBD and NXF1-NTF2 both interact with the core fragment of EBOV NP. (A) Structural organization of EBOV NP. Numbers indicate amino acid positions. (B) Coimmunoprecipitation of NXF1-RBD and NXF1-NTF2 with NP mutants. 293T cells were transfected with plasmids encoding either flag/HA-NXF1-RBD or flag/HA-NXF1-NTF2, together with plasmids encoding different myc-tagged NP constructs, as indicated. Cells were lysed at 48 h posttransfection, and NXF1 domains were precipitated with anti-flag antibodies. Input and precipitates were subsequently analyzed via SDS-PAGE and Western blot with detection of the NXF1 domains and NP using anti-HA and anti-myc antibodies, respectively. Shown are representative results from four independent experiments.

between the NTF2 domain and NP-ΔC-tail seems to be weaker than the NTF2:NP interaction. Furthermore, the CTD of EBOV NP was not sufficient to mediate interaction with either the NXF1-RBD or the NTF2 domain.

NP-K160A.R171A.R174A shows reduced RNA binding while still promoting IB formation. We have previously established that RNA binding by NXF1 weakens its interaction with EBOV NP and that single-stranded RNA and NP seem to compete for interaction with NXF1 (20). To analyze the effect of RNA binding by NP on its interaction with NXF1, we generated an RNA binding-deficient NP by introducing three mutations in the NP core fragment that have been previously identified to be involved in

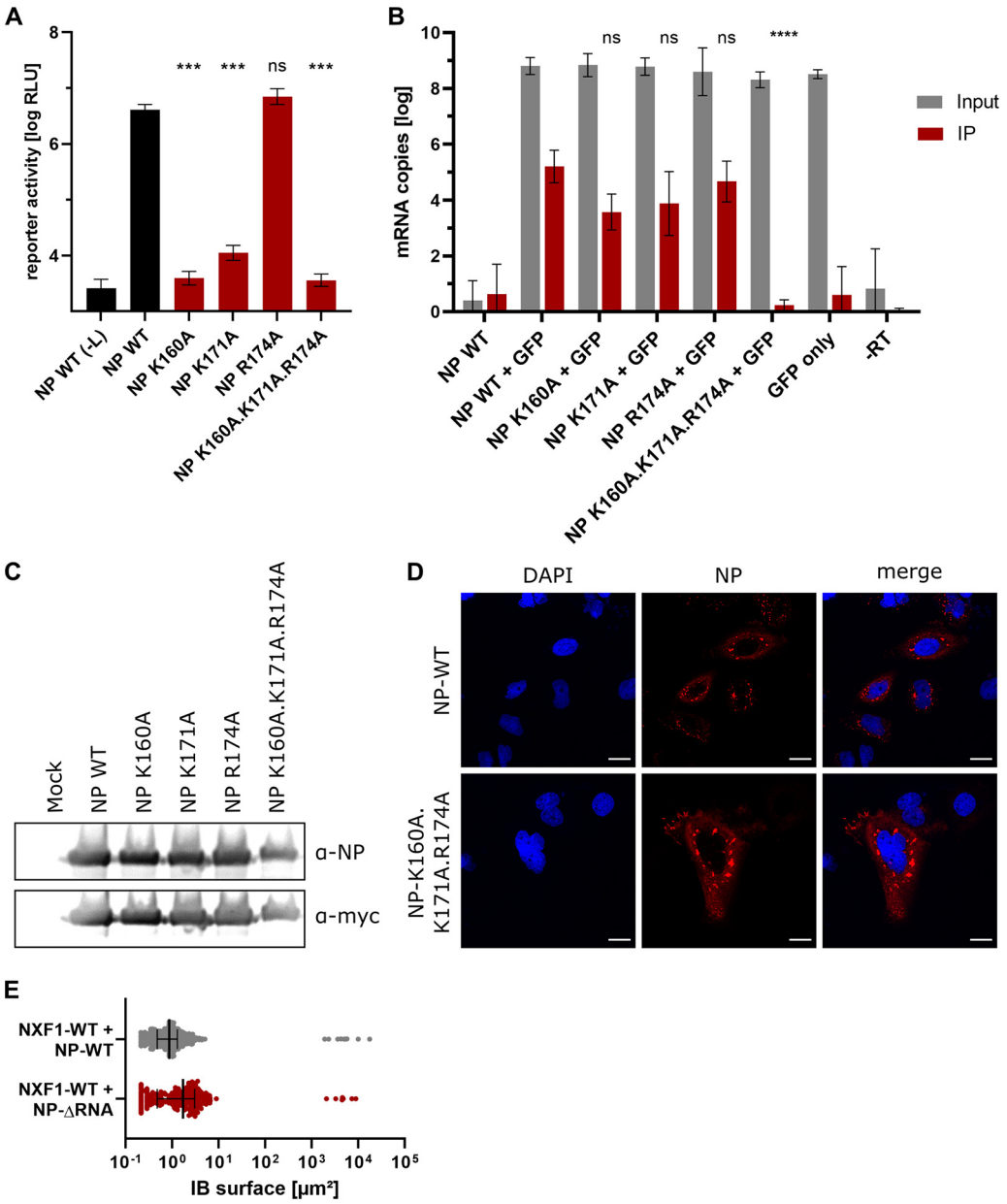

FIG 7 Characterization of RNA binding-deficient EBOV NP. (A) Minigenome assay. 293T cells were transfected with plasmids encoding T7 polymerase, the viral proteins L, VP30, and VP35, and the EBOV minigenome, as well as plasmids encoding the different NP constructs indicated. As a negative control, the viral polymerase was omitted (–L). At 48 h posttransfection, cells were harvested, and the reporter activity was determined. (B) RNA coIP. 293T cells were transfected with plasmids encoding the different myc-tagged NP constructs as well as GFP. At 2 days posttransfection, cells were lysed, and NP was precipitated using anti-myc antibodies. Coprecipitated RNA was isolated from the samples, and GFP-mRNA was subsequently quantified via RT-qPCR. Shown are the results of three independent experiments. Asterisks indicate *P* values from one-way ANOVA (ns, $P > 0.05$; ***, $P \leq 0.001$; ****, $P \leq 0.0001$). (C) Expression of the different NP mutants. 293T cells overexpressing the different myc-tagged NP constructs were harvested at 48 h posttransfection, and the cell lysates were analyzed via SDS-PAGE and Western blotting. NP was detected using both anti-NP and anti-myc antibodies. (D) Inclusion body formation. Huh7 cells overexpressing either NP-WT or NP-K160A.K171A.R174A were fixed and permeabilized at 48 h posttransfection. NP (shown in red) was detected using anti-myc antibodies, and nuclei (shown in blue) were stained with DAPI. Cells were analyzed by confocal laser scanning microscopy. Scale bars, 20 μm. (E) Quantification of inclusion body size. The surface areas of IBs with a surface area of >0.2 μm^2 were determined using the Arivis Vision 4D software.

RNA binding (29, 31). To characterize these mutants, their functionality was first assessed using an EBOV minigenome assay (Fig. 7A). This assay showed that K160 and R171 are both essential for RNA synthesis and/or protein expression, since the reporter activity was comparable to the negative control lacking the viral polymerase (–L) if

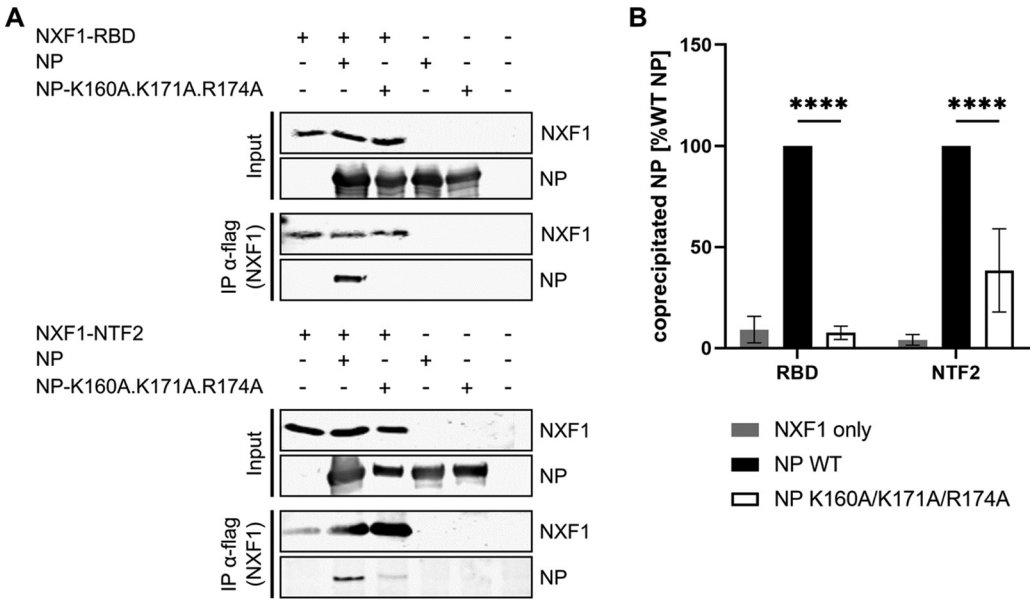

FIG 8 NXF1-RBD but not NXF1-NTF2 interacts with the RNA binding cleft of NP. (A) Coimmunoprecipitation of NXF1 and NP variants. Coimmunoprecipitation of flag/HA-tagged NXF1-RBD or NXF1-NTF2, together with EBOV NP or an RNA binding-deficient mutant of NP, was performed with cell lysates from 293T cells at 48 h posttransfection. Precipitation of NXF1 was performed using anti-flag antibodies, and input and precipitates were analyzed via SDS-PAGE and Western blotting using anti-HA and anti-myc antibodies for the detection of NXF1 and NP, respectively. (B) Quantification of coprecipitated NP. Signal intensities for NP detected via Western blot were determined, and the amounts of coprecipitated NP in relation to NP-WT were calculated. Shown are the results of four independent experiments. Asterisks indicate *P* values from two-way ANOVA (****, $P \leq 0.0001$).

either of these amino acids was mutated. In contrast, the mutation at position R174 showed no impact on RNA synthesis. Finally, NP harboring all three mutations resulted in levels of reporter activity comparable to the negative control (–L). To assess whether this phenotype was accompanied by a loss of RNA binding by NP, we performed coIPs with EBOV NP and GFP-mRNA, since NP is known to bind to cellular mRNAs in the absence of viral RNA (33, 34). The amount of coprecipitated RNA was subsequently quantified via RT-qPCR (Fig. 7B). Using this approach, we could demonstrate that NP-K160A and NP-R171A both show some residual RNA binding, since they were still able to coprecipitate GFP-mRNA, albeit in reduced amounts. In contrast, NP harboring all three mutations completely lost its ability to bind RNA, as the amount of precipitated GFP-mRNA in the respective sample was comparable to that detected in the negative controls (wild-type NP only or GFP mRNA only). To ensure that the observed phenotype was not based on differences in the expression of the different NP constructs, their expression levels were assessed via SDS-PAGE and Western blotting. These experiments showed that all NP constructs used in these experiments were expressed to a similar extent (Fig. 7C).

To further assess the functionality of the RNA binding-deficient EBOV NP (K160A.R171A.R174A), we analyzed whether the introduced mutations have an impact on the formation of NP-induced IBs. When comparing wild-type and RNA binding-deficient NPs, we observed that NP-K160A.R171A.R174A was still able to form IBs, although these were larger in size compared to those formed by wild-type NP (Fig. 7D and E).

NXF1-RBD interacts directly with the RNA binding cleft of NP. We next used the RNA binding-deficient NP to analyze the importance of NP RNA binding for its interaction with NXF1 (Fig. 8). When performing coIPs with the RBD of NXF1, we could show that RNA binding-deficient NP did not coprecipitate together with NXF1, indicating that the three mutations introduced to abolish RNA binding by NP also resulted in a loss of interaction with NXF1-RBD (Fig. 8). In contrast, coIP of NXF1-NTF2 with RNA binding-deficient NP showed a reduced, but still detectable amount of coprecipitated NP (Fig. 8). This suggests

that the RNA-binding cleft of NP is beneficial but not absolutely required for interaction with NXF1-NTF2 and that the NTF2 domain interacts with a different region of NP than the RBD.

Loss of RNA binding by NP leads to the accumulation of NXF1 in IBs. We have previously shown that NXF1 is present only at low levels in EBOV IBs, while RNA binding-deficient mutants of NXF1 (e.g., NXF1-ΔRBD) accumulate in these structures, indicating shuttling of NXF1-WT in and out of IBs, with export being triggered in response to RNA binding (20). To assess whether only RNA binding of NXF1 influences its localization and accumulation in EBOV IBs or whether RNA binding by NP also plays a role, we performed coimmunofluorescence analyses with wild-type and RNA binding-deficient versions of both NXF1 and NP (Fig. 9). Using this approach, we could confirm that NXF1-WT localizes only weakly in NP-WT-derived IBs, whereas RNA binding-deficient NXF1 (NXF1-ΔRBD) accumulated in these structures (Fig. 9A). Importantly, when the IBs were formed by RNA binding-deficient NP, we observed an accumulation of both wild-type NXF1 and NXF1-ΔRBD in IBs, with the latter showing the strongest phenotype (Fig. 9). This indicates that the loss of RNA binding by both NXF1 and NP still allows NXF1 to enter IBs, but seems to efficiently block NXF1 from leaving these structures again, and that both the RNA binding ability of NXF1 and NP play a role in NXF1 escaping from IBs.

NXF1 is also required by other negative-sense RNA viruses. To assess whether the function of NXF1 in the EBOV life cycle is conserved among cytoplasmically replicating negative-sense RNA viruses, we performed minigenome assays for other selected negative-sense RNA viruses in the context of siRNA-mediated knockdown of NXF1. First, we analyzed the importance of NXF1 for another filovirus, the recently discovered Lloviu virus (LLOV) (Fig. 10A) (35). LLOV minigenome assays in cells treated with NXF1-siRNAs showed a similar reduction in reporter activity to that observed with the EBOV minigenome assay (Fig. 2B), demonstrating that NXF1 is also required for RNA synthesis and/or protein expression of LLOV. We then expanded the analysis to other hemorrhagic fever causing negative-sense RNA viruses from outside the filovirus family. Minigenome assays for Junín virus (JUNV), which has also been suggested to replicate in cytoplasmic IBs (36), showed a similar phenotype to that observed with the LLOV and EBOV minigenome assays in cells treated with NXF1-siRNAs (Fig. 10B). In contrast, Crimean-Congo hemorrhagic fever virus (CCHFV) minigenome assays in cells treated with NXF1-siRNAs resulted in reporter activity levels comparable to cells treated with a negative-control siRNA (Fig. 10C), indicating that NXF1 is not required for RNA synthesis or protein expression of CCHFV and also that the observed phenotype is specific for certain viruses, rather than being a product of the experimental system itself.

DISCUSSION

In previous studies examining the role of NXF1 in the EBOV life cycle we have shown that NXF1 is necessary for a step downstream of viral transcription (20, 21). Based on what is known about the functions and characteristics of NXF1 in the nucleus, we proposed a model in which NXF1 exports EBOV mRNAs from IBs (20). We now demonstrate that NXF1 interacts with authentic viral mRNAs and that NXF1 is dispensable for the translation of *in vitro*-transcribed viral mRNA analogues, pinpointing the function of NXF1 to a step in the virus life cycle downstream of viral mRNA synthesis but upstream of viral mRNA translation. In this context, it has to be noted that we cannot completely exclude that the *in vitro*-transcribed viral mRNA might have subtly different physical properties than mRNAs generated during viral infection, such as different posttranscriptional modifications, although, importantly, they both are nonspliced, capped, and poly(A) tailed. Thus, these additional findings strongly support the previously proposed role of NXF1 in export of mRNA from IB for translation by ribosomes. Aside from RNA transport/export from IBs, these data would also be consistent with a role of NXF1 in stabilizing viral mRNAs. However, while in the cell NXF1 is well known to play an essential role in the export of mRNA out of the nucleus (21), no

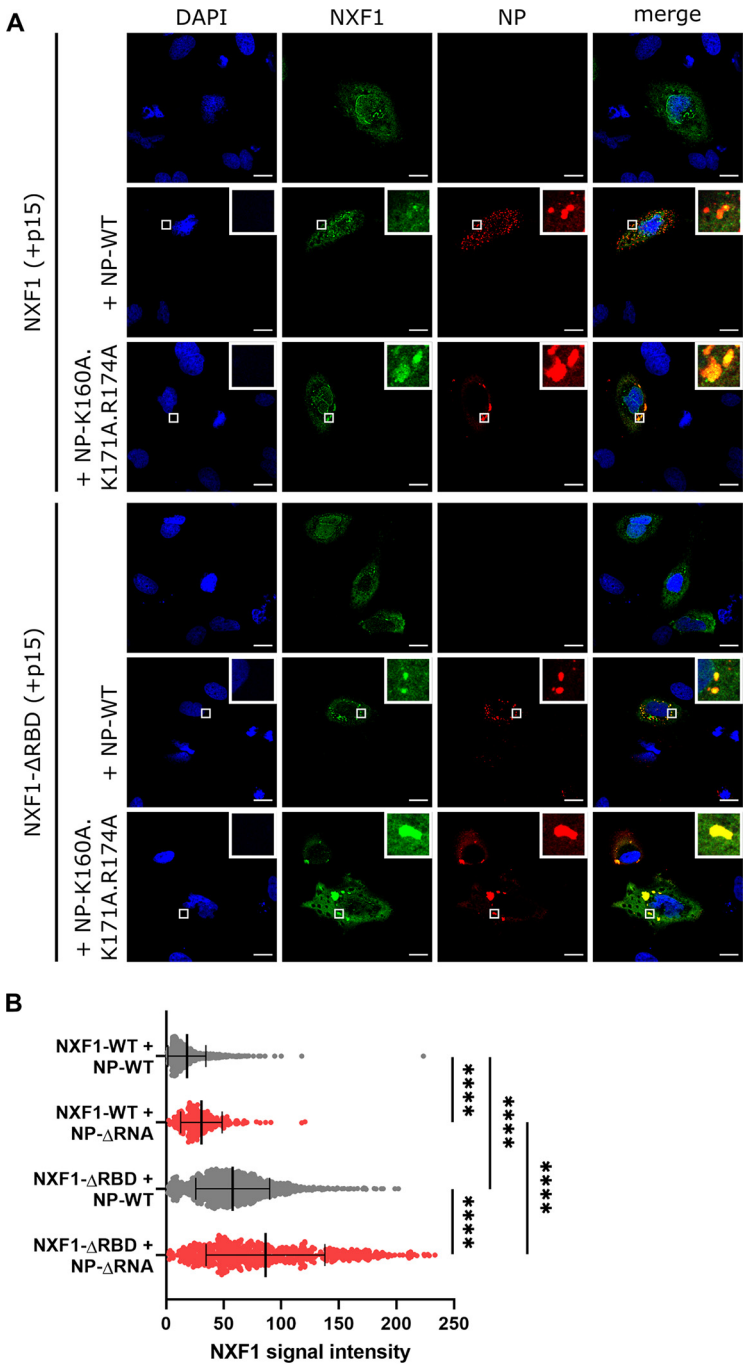

FIG 9 NXF1 requires the RNA-binding capability of EBOV NP to exit NP-derived IBs. (A) Coimmunofluorescence analysis. Huh7 cells were transfected with plasmids encoding flag/HA-tagged NXF1-WT or NXF1-ΔRBD, together with pCAGGS-p15, as well as plasmids encoding myc-tagged EBOV NP-WT or NP-K160A.K171A.R174A, as indicated. At 2 days posttransfection, cells were fixed and permeabilized. Flag/HA-NXF1 (shown in green) was detected using an anti-flag antibody and NP (shown in red) was detected with an anti-myc antibody. Nuclei (shown in blue) were stained with DAPI, and cells were analyzed by confocal laser scanning microscopy. Scale bars indicate 20 μm, and insets show magnifications of the indicated areas. (B) Quantification results. The mean fluorescence intensity of NXF1 in IBs was determined using the Arivis Vision 4D software. Shown are all values for IBs with a surface area of $>$0.2 μm^2. Asterisks indicate *P* values from one-way ANOVA (****, $P \leq 0.0001$).

function in mRNA stability has so far been described, and also in the context of other viral infections NXF1 is not known to be involved in the translation or stability of viral mRNAs (22, 24, 25, 37, 38). Further, and even more importantly, if mRNA stability would

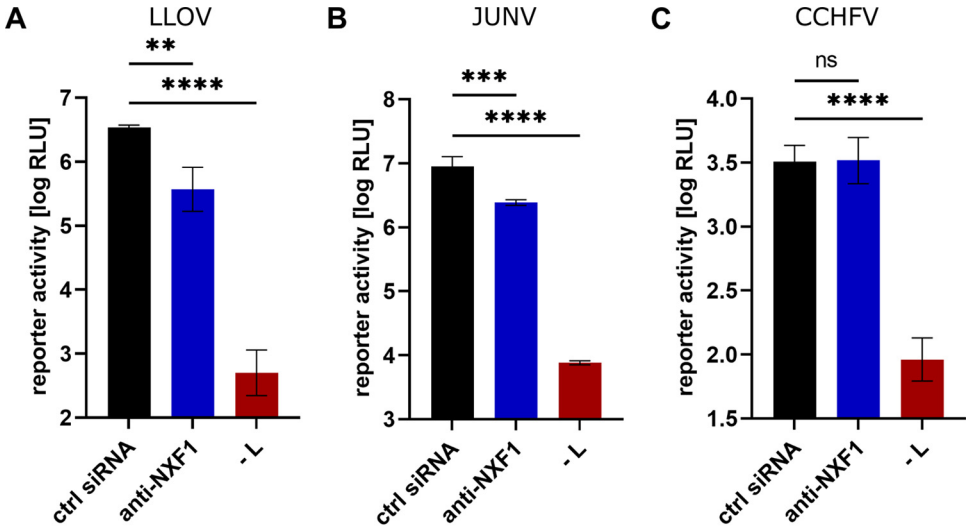

FIG 10 NXF1 is also necessary for protein expression of LLOV and JUNV but not CCHFV. 293T cells were reverse transfected with siRNAs targeting NXF1 or a negative-control (ctrl) siRNA. At 2 days posttransfection, cells were transfected with all components for a LLOV (A), JUNV (B), or CCHFV (C) replication-competent minigenome assay. As a control, the viral polymerase was omitted (–L). After another 2 days, cells were harvested, and the reporter activity was measured. The means and standard deviations of three (B) or four (A and C) independent experiments are shown. Asterisks indicate *P* values from one-way ANOVA (ns, $P > 0.05$; **, $P \leq 0.01$; ***, $P \leq 0.001$; ****, $P \leq 0.0001$).

be affected, this would result in a decrease in the number of viral mRNAs after NXF1 knockdown, which was clearly not the case (20).

Further support for a role of NXF1 in the export of viral mRNAs from IBs comes from details regarding the molecular mechanism by which NXF1 exerts its function in the EBOV life cycle, which show some striking similarities to the cellular function of NXF1. To assess this mechanism, we used well-established NXF1 deletions or single domains to further dissect aspects of the function of NXF1 that we had previously established in the context of full-length NXF1. In particular, we demonstrate that both the RBD and the NTF2 domain of NXF1 interact with different sites on EBOV NP. However, since our coIP studies were performed with whole-cell lysates (i.e., rather than purified proteins), we cannot exclude a role for bridging proteins in this interaction. Nonetheless, these two domains within NXF1 are known to form an intramolecular interaction, which has to be disrupted in order to allow cellular mRNA binding by NXF1 as a prerequisite for its transport function (23). Thus, the interactions between NXF1 and two different sites on NP could serve the same purpose as the interaction between NXF1 and the TREX components Aly and THOC5, i.e., the disruption of the intramolecular interaction between the RBD and NTF2 domains and the resulting conformational activation of NXF1 (23). Further, our data indicate that the RNA binding ability not only of NXF1 but also of NP is important for the export of NXF1 from IBs, since disrupting either results in an accumulation of NXF1 in IBs. This observation can be explained by loading of NXF1 with viral mRNA via a handover mechanism from NP reminiscent of the handover in the nucleus that results in the loading of NXF1 with cellular mRNAs (39–42). Based on these features, mRNA export from IBs would appear to closely resemble the mechanisms used during nuclear mRNA export, since both involve the conformational activation of NXF1 through disruption of the RBD-NTF2 interaction and a handover of mRNA from NP (or cellular export adaptors) to NXF1 (23, 39–42). Interestingly, we could show that the amino acids in the RNA binding cleft of NP that are essential for RNA binding are also required for interaction with the RBD of NXF1, indicating that the RBD can bind directly within the RNA binding cleft of NP. Such an interaction might result in a displacement of RNA from these amino acids and trigger the handover of the mRNA from NP to the RBD of NXF1.

Although the RBD of NXF1 clearly interacts with NP, our data show that this domain is not sufficient for recruitment into IBs, and we have previously shown that it is also not required for this recruitment (20). In contrast, the two C-terminal domains of NXF1, the NTF2 domain and the UBA domain, are both sufficient to promote recruitment of NXF1 into EBOV IBs. In the cellular context these two domains mediate the interaction of NXF1 with nucleoporins through multiple low-affinity interactions with FG repeats (37, 43, 44). Given that the IBs of a number of negative-sense RNA viruses are liquid organelles (17, 18, 45) and that EBOV IBs also show at least some of the features characteristic for such organelles (12), it is possible that similar low-affinity interactions through the NTF2 and UBA domains facilitate the recruitment of NXF1 into IBs. Alternatively, given that the NTF2 domain of NXF1 also interacts with NP, NXF1 could also be recruited into IBs through this interaction, although this does not explain the recruitment of the UBA domain.

In this context, it is important to note that colocalization and interactions as detected by coIP experiments are not necessarily equivalent. Indeed, the coIP data allow us to assess which domains of NP and NXF1 can interact with each other if given the chance, i.e., without any localization bias. The colocalization data on the other hand allow us to examine how NXF1 is recruited into inclusion bodies, which is a prerequisite for its interaction with NP. However, colocalization does not necessarily require physical interaction. Specifically, in the case of liquid organelles, proteins or domains can be recruited into these structures by multiple weak interactions or based on their biophysical properties alone (which are then highly concentration as well as salt and pH dependent). As such, these kinds of interactions cannot be detected in coIP, which is designed for the detection of relatively stable protein-protein interactions.

The importance of the NTF2 and UBA domains for recruitment of NXF1 into IBs and the role of the RBD and the NTF2 domain for interacting with EBOV NP, and in case of the RBD also with viral mRNA (20), then explains why NXF1 mutants that lack any of these three domains (or a combination of them) cannot rescue siRNA-mediated knockdown of NXF1. Accordingly, the RRM domain, which was shown to be dispensable for interaction of NXF1 with both mRNA and NP (20), as well as for the localization of NXF1 in IBs, is also dispensable for the function of NXF1 in viral protein expression. However, the LRR domain, which did not show an interaction with NP or recruitment into IBs, is still required for the function of NXF1 in EBOV protein expression. While the reason for this remains unclear, one possible explanation might be that the LRR domain, which is much longer than the dispensable RRM domain and flanked by flexible linker regions (21, 44), might be important to ensure a correct spacing of the RBD and NTF2 domain and/or to maintain a certain degree of flexibility of these domains with respect to each other that is necessary for proper conformational activation of NXF1.

Based on our data, we now propose an updated model in which the NTF2 and UBA domains direct the localization of NXF1 to EBOV IBs (Fig. 11). Within these structures, NP can further recruit NXF1 towards the nascent mRNA during viral transcription via its interaction with the NTF2 domain. This NP-NTF2 interaction then leads to disruption of the intramolecular interaction between the NTF2 domain and the RBD of NXF1, so that the now freed RBD can in turn interact with the RNA binding cleft of NP. This interaction triggers a handover of the mRNA from NP to NXF1, thereby displacing NP from the mRNA and allowing NXF1 to export the viral mRNA from IBs.

This model would not only explain how EBOV mRNAs escape the environment of IBs where RNA binding proteins such as NP, VP30, and VP35 are highly abundant (14, 46) but might also provide an explanation for how EBOV prevents the encapsidation of mRNAs by NP. While it has been proposed that the 5′ cap structure prevents EBOV NP from encapsidating mRNA, previous studies have shown that NP is indeed able to encapsidate cellular mRNAs despite their 5′ cap structure when there are no viral RNA species present (33, 34), and our results also clearly show this to be the case for GFP-mRNA, as well as for VP40-mRNA in EBOV-infected cells. A handover of viral mRNA

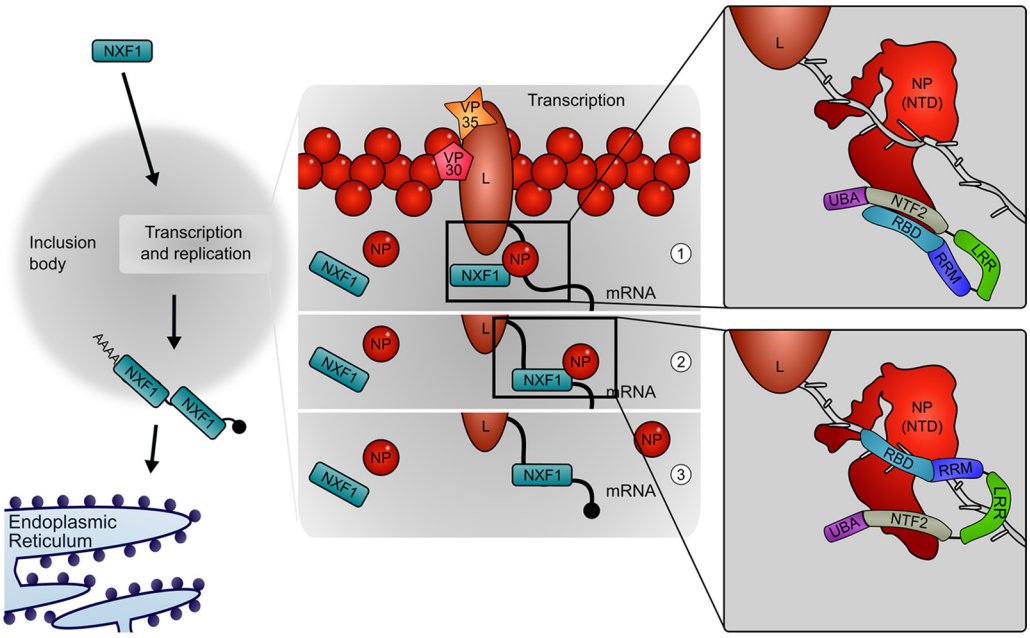

FIG 11 Model for the role of NXF1 in the EBOV life cycle. NXF1 localizes in EBOV IBs, where NP recruits it towards the nascent mRNA during transcription via the NP-NTF2 interaction (subpanel 1). This leads to the disruption of the RBD-NTF2 interaction in NXF1 so that the RBD can interact with the RNA-binding cleft of NP, which triggers the handover of the mRNA from NP to NXF1 (subpanel 2). Through the handover of the mRNA, NP is displaced from the mRNA (subpanel 3), and NXF1 can then export the viral mRNA from the IBs towards ribosomes for translation.

from NP to NXF1, the displacement of NP from the mRNA, and subsequent export out of the NP-enriched IBs would provide a solution to this problem.

Importantly, many other negative-sense RNA viruses are also known to replicate in cytoplasmic IBs and thus face the same challenges. Indeed, analysis of the requirement of NXF1 as a host cell factor revealed that it is not only necessary for the EBOV life cycle but also for the related filovirus LLOV, as well as the arenavirus JUNV, which, like filoviruses, has been suggested to replicate in cytoplasmic IBs (36). In contrast, reporter activity in the CCHFV minigenome assay remained unaffected by siRNA-mediated knockdown of NXF1. This not only confirms the specificity of the observed effects, but is also consistent with the fact that bunyaviruses such as CCHFV replicate in cytoplasmic, but membranous Golgi compartment-associated replication organelles (47), rather than membraneless liquid organelles. In addition, it is believed that translation of bunyaviral mRNAs occurs cotranscriptionally, which would make mRNA export redundant (48). Consequently, an mRNA export protein such as NXF1 would not be expected to be required for the life cycle of CCHFV. Therefore, these data, when taken together, also support a model in which NXF1 is required for viral mRNA export from IBs, since this process would be expected to be important for the life cycles of filo- and arenaviruses, which replicate in these types of structures (12, 36), but not for bunyaviruses, which replicate in membranous replication organelles (47). Further investigations of the specific function of NXF1 in the life cycle of JUNV, as well as other negative-sense RNA viruses that replicate in cytoplasmic IBs, will help to further substantiate whether NXF1-mediated viral mRNA export from IBs is indeed a conserved feature among such viruses, which would make this a promising target for broadly acting antiviral therapeutics.

MATERIALS AND METHODS

Cells. Human embryonic kidney (HEK293T) cells (Collection of Cell Lines in Veterinary Medicine, CCLV-RIE 1018) and human hepatocarcinoma (Huh7) cells (kindly provided by Stephan Becker, Philipps University, Marburg, Germany) were maintained in Dulbecco modified Eagle medium (DMEM; Thermo Fisher Scientific) supplemented with 100 U/mL penicillin and 100 μg/mL streptomycin (Thermo Fisher Scientific), 1$\times$ GlutaMAX (Thermo Fisher Scientific), and 10% fetal bovine serum. All cells were grown at 37°C and 5% CO_2.

Plasmids. Expression plasmids for T7 polymerase, the T7-driven EBOV monocistronic minigenome (pT7-1cis-vRNA-hrluc), the Pol II-driven replication-deficient minigenome (pCAGGS-1cis-vRNA-nluc-RdM), the EBOV RNPs and flag/HA-tagged NXF1 constructs have been described previously (4, 20, 49). Also, the plasmids for the Pol II-driven LLOV monocistronic minigenome (pCAGGS-1cis-LLOV-vRNA-hrluc) and the LLOV RNPs, the T7-driven JUNV minigenome (pAMP-JUNV-S-mg-nluc-1L/2L) and the JUNV RNPs, as well as the T7-driven CCHFV minigenome (pT7ribo-10200-L-HHR-rluc) and the CCHFV RNPs, have been described previously (50–53). The expression plasmid for dominant-negative protein kinase R (DN-PKR; pI.18-HA-PKRdelE7) has also been described (54). The plasmid for the *in vitro* transcription of viral mRNA (pT7-EBOV-1cis-nluc-ΔldrΔtrl) was cloned from a classical T7-driven minigenome expressing nanoluciferase as a reporter (pT7-1cis-vRNA-nluc [28]) by deleting the leader and trailer regions. For the expression of C-terminally myc-tagged EBOV NP, the myc tag was added to the NP open reading frame via PCR and subcloned into pCAGGS. All deletion mutants of NP were generated by amplification of the respective part of the NP gene by PCR and ligation into pCAGGS-myc. Point mutations for the generation of RNA binding-deficient NP were inserted into pCAGGS-EBOV-NP-myc via recombinant PCR. For complementation of the siRNA-mediated knockdown of NXF1, six silent mutations were introduced within the siRNA binding site in the previously described pCAGGS-flag/HA-NXF1 (or mutant versions) (20). To this end, every third nucleotide was exchanged to correspond to the next most frequently used codon for each encoded amino acid, resulting in the sequence 553-CGG AGA ATC TCC ATT ATT-570 (positions are nucleotide positions in the NXF1 open reading frame). Detailed cloning strategies are available on request.

Antibodies. The anti-flag antibody (mouse anti-flag, clone M2; Sigma-Aldrich, catalog no. F1804) was used for immunofluorescence analyses (IFA) and coimmunoprecipitation (coIP). The anti-c-*myc* antibody (rabbit; Thermo Fisher Scientific, catalog no. PA1-981) was used for immunofluorescence and Western blot analyses, and for the detection of HA-tagged proteins in Western blot analyses the anti-HA antibody (chicken; Abcam, catalog no. ab9111) was used. Primary antibodies against EBOV NP (rabbit; catalog no. 0301-012) were purchased from IBT Bioservices. Secondary antibodies against rabbit (Alexa Fluor 790, goat anti-rabbit, Dianova; catalog no. 111-655-144) and chicken (Alexa Fluor 680, donkey anti-chicken; Dianova, catalog no. 703-625-155) were used for detection in Western blot analyses, while secondary antibodies against mouse (Alexa Fluor 488, goat anti-mouse; Thermo Fisher Scientific, catalog no. A-11029) and rabbit (Alexa Fluor 568, goat anti-rabbit; Thermo Fisher Scientific, catalog no. A-11036) were used for IFA.

Coimmunoprecipitation in EBOV-infected cells. 293T cells in a six-well format were infected with rgEBOV at a multiplicity of infection of 2. At 1 h postinfection, the cells were transfected with the plasmids encoding flag/HA-tagged NXF1, NXF1-ΔRBD, or NP using Transit LT-1 (Mirus Bio) according to the manufacturer's instructions. At 2 days postinfection, cells were subjected to coIP as described previously (20). Briefly, cells were lysed using a 1% NP-40 buffer with protease inhibitor (cOmplete; Roche) at 4°C overnight, and cleared preimmune lysates were subjected to coIP using anti-flag-coupled magnetic beads (Protein G Dynabeads; Thermo Fisher Scientific) for 10 min at room temperature. The beads were washed three times with phosphate-buffered saline (PBS) containing 0.02% Tween 20 and resuspended in PBS. A portion of the cleared preimmune lysate representing 17.5% of the sample subjected to immunoprecipitation (IP) was used as an input control. TRIzol LS (Thermo Fisher Scientific) was added to IP and input samples before removal from the BSL4 laboratory. All experiments involving infectious EBOV were performed in the BSL4 laboratory of the Friedrich-Loeffler-Institut according to approved standard operating procedures.

***In vitro* transcription of viral mRNA.** For the *in vitro* transcription of viral mRNA, the template (pT7-EBOV-1cis-nluc-ΔldrΔtrl) was linearized using XhoI (New England Biolabs) before mRNA synthesis was performed using a HiScribe T7 ARCA mRNA kit (with tailing; New England Biolabs) according to the manufacturer's instructions.

siRNA knockdown in the EBOV minigenome assay. For siRNA knockdown, 293T cells were reverse transfected with 12 pmol anti-L siRNA (5′-UUU AUA UAC AGC UUC GUA CUU-3′) or predesigned silencer select siRNAs (NXF1: s20532, Negative Control siRNA#2; Thermo Fisher Scientific) using Lipofectamine RNAiMax (Thermo Fisher Scientific) according to the instructions of the manufacturer in 12-well plates. To assess the impact of NXF1 on viral translation, the cells were transfected with 500 ng of either minigenome-derived mRNA (nluc) or Firefly mRNA (RiboPro) using Lipofectamine MessengerMAX (Thermo Fisher Scientific) according to the manufacturer's instructions 2 days after the siRNA transfection. As a negative control, no mRNA was added (–mRNA). Further, as a control for the successful knockdown of NXF1, siRNA-treated cells were also transfected with the plasmids encoding the minigenome (pT7-EBOV-1cis-vRNA-hrluc), the T7 polymerase, and the RNPs (NP, L, VP35, and VP30), as well as a firefly luciferase transfection control. For the complementation of siRNA-mediated knockdown of NXF1, the NXF1-depleted cells were transfected with all components required for the replication-deficient minigenome as previously described (49), together with different NXF1 constructs harboring mutations in the siRNA binding site. The plasmid amounts for the NXF1 mutants used in this assay were adjusted to ensure equal expression levels (corresponding to 250 ng of pCAGGS-flag/HA-NXF1-ΔsiRNA), as judged using the same workflow and Western blot analysis 2 days posttransfection with an anti-flag antibody. Two days after the second transfection, cells were lysed for 10 min in 1× Lysis Juice (PJK), and the lysates were cleared by centrifugation (3 min, 10,000 × *g*, room temperature). Then, 40 μL of the cleared lysate was added to 40 μL of either Renilla Glo Juice or Beetle Juice (both PJK) or NanoGlo luciferase assay reagent (Promega) in opaque 96-well plates. For measurement of luminescence, a GloMax Multi (Promega) multiplate reader was used. Minigenome reporter activity or viral mRNA reporter activity was normalized to firefly luciferase activities.

coIP of viral proteins. coIP was performed as described previously (20). Briefly, 293T cells were transfected with the plasmids encoding for flag/HA-tagged NXF1 constructs and myc-tagged NP-constructs. At 48 h posttransfection, the cells were harvested and lysed using 1% NP-40 buffer with protease inhibitor. For the coIP results depicted in Fig. 3 and Fig. 6 100 mg/mL RNase A (Macherey-Nagel) were added to the lysis buffer. Preimmune lysates were incubated with anti-flag coupled magnetic beads (Protein G Dynabeads; Thermo Fisher Scientific) for 10 min at room temperature. Beads were washed with PBS containing 0.02% Tween 20 and resuspended in SDS-PAGE sample buffer. One-sixth of the preimmune lysate (representing 20% of the IP sample) was subjected to acetone precipitation. IP and input samples were subjected to SDS-PAGE and Western blotting, and membranes were analyzed using a LI-COR Odyssey CLx. The signal intensities were quantified using LI-COR Image Studio Lite v5.2.

Immunofluorescence analysis. Huh7 cells were seeded in 12-well plates onto coverslips and transfected on the next day with 500 ng of pCAGGS-flag/HA-NXF1 (or other NXF1 constructs, as indicated) or 500 ng of pCAGGS-p15, as well as 500 ng pCAGGS-EBOV-NP-myc (or pCAGGS-EBOV-NP-K160A.K171A.R174A-myc). Transfections were performed using polyethylenimine (Sigma-Aldrich) according to the manufacturer's instructions. Fixation of the cells was performed at 48 h posttransfection with 4% paraformaldehyde (Carl Roth) in DMEM for 20 min. Afterward, the cells were treated with 0.1 M glycine in PBS and permeabilized using 0.1% Triton X-100 in PBS. Cells were blocked with 10% FCS in PBS for 45 min before incubation with primary antibody diluted in 10% FCS in PBS (mouse anti-flag, 1:2,500; rabbit anti-myc, 1:1,500) for 1 h at room temperature. Secondary antibodies were also prepared in 10% FCS in PBS (Alexa Fluor 568 anti-rabbit, 1:1,500; Alexa Fluor 488 anti-mouse, 1:1,200), and staining was performed for 1 h at room temperature. Cells were rinsed with PBS and water before being mounted with ProLong Diamond Antifade mountant with DAPI (4′,6′-diamidino-2-phenylindole; Thermo Fisher Scientific). Slides were analyzed by confocal laser scanning microscopy using a Leica SP5 (63× oil immersion objective).

Confocal records were quantified using Arivis Vision4D 3.4 software. Each fluorescence channel was denoised using the Discrete Gaussian filter. The cells were segmented using an Intensity Threshold Segmenter with the percentile thresholding method set to 80% on the NXF1 channel to eliminate negative cells. The IBs were detected using the Automatic Small Objects detection method (Blob finder segmentation) with a diameter set to 1 μm, a probability threshold of 10%, and a split sensitivity of 50%. The fluorescence intensity of individual IBs in each channel was quantified. At least 5 views from each analyzed combination were quantified, and only IBs with a surface area of >0.2 μm^2 were selected for downstream analysis.

RNA coIP. For coIP of GFP-mRNA, 293T cells were transfected with pCAGGS-eGFP (250 ng) and the plasmids for the expression of myc-tagged NP mutants (1500 ng) using Transit LT-1 (Mirus Bio) according to the manufacturer's instructions. As controls, either the green fluorescent protein (GFP) or NP plasmid was omitted. The coIP procedure was performed at 48 h posttransfection as described above for the protein coIPs, but the beads were resuspended in 100 μL of PBS instead of SDS-PAGE sample buffer to allow for RNA isolation.

RNA isolation and RT-qPCR. RNA isolation from input and IP samples was performed using TRIzol (Thermo Fisher Scientific) or TRIzol LS in case of BSL4 samples according to the manufacturer's instructions. Briefly, 500 μL of TRIzol or 750 μL of TRIzol LS was added to the samples, followed by incubation for 5 min at room temperature. After the addition of 100/200 μL of chloroform (Carl Roth), samples were vortexed vigorously and centrifuged at 12,000 $\times$ *g* for 15 min and 4°C. The aqueous phase was transferred to a new tube, and 2 μL of GlycoBlue (Thermo Fisher Scientific) and 250 or 500 μL of ice-cold isopropanol was added before incubation at −20°C for at least 30 min. RNA was pelleted and washed with ethanol before resuspension in nuclease-free water. GFP RNA samples were treated with Turbo DNase (Thermo Fisher Scientific) according to the manufacturer's instructions. The mRNA was reverse transcribed using an oligo(dT) primer with RevertAid reverse transcriptase (Thermo Fisher Scientific) according to the manufacturer's instructions. The resulting cDNA was analyzed via qPCR using PowerUp SYBR green master mix (Thermo Fisher Scientific) according to the manufacturer's instructions with either GFP-specific primers [GFP(+), 5′-CTT GTA CAG CTC GTC CAT GC-3′; GFP(–), 5′-CGA CAA CCA CTA CCT GAG CAC-3′] (20) or VP40-specific primers [VP40(+), 5′-CAT GGT GAG GTC TCC TGG AG-3′; VP40(–), 5′-GAC CGG TAA GAA GGT GAC TTC-3′].

siRNA knockdown in LLOV, JUNV, and CCHFV minigenome assays. The workflow for siRNA knockdowns in context of minigenome assays for other negative-sense RNA viruses was similar to that described above for EBOV. 293T cells were reverse transfected with siRNAs targeting either NXF1 or a negative-control siRNA. Two days after the siRNA transfection, cells were transfected with all the components necessary for the respective minigenome assay, as described above, using Transit LT-1 (50–53). Briefly, for the LLOV minigenome assay, cells were transfected with plasmids encoding LLOV NP, VP30, VP35, L, the Pol II-driven LLOV minigenome, and firefly luciferase as a transfection control. For the JUNV minigenome assay, cells were transfected with the plasmids encoding the T7 polymerase, the T7-driven JUNV minigenome (pAMP-JUNV-S-mg-nluc-1L/2L), JUNV L, NP, firefly luciferase, and DN-PKR. Similarly, for the CCHFV minigenome assay, cells were transfected with the plasmids encoding the T7 polymerase, the T7-driven CCHFV minigenome (pT7ribo-10200-L-HHR-rluc), CCHFV L, N, firefly luciferase, and DN-PKR. As a control in all three assays, the viral polymerase (L) was omitted. Two days after the minigenome transfection, cells were lysed for 10 min in 1× Lysis Juice. Lysates were cleared by centrifugation for 3 min at 10,000 $\times$ *g*, and 40 μL of cleared lysate was added to 40 μL of either Beetle Juice (PJK), Renilla Glo Juice (PJK), or Nano-Glo luciferase assay reagent (Promega) in opaque 96-well plates. The luminescence was subsequently measured using a GloMax Multi microplate reader (Promega). Reporter activities obtained for the minigenome reporter were normalized to control luciferase (firefly) activity.

Statistical analyses. One-way analysis of variance (ANOVA) with Dunnett's multiple-comparison test (Fig. 1, 2, 5, 7, and 10) or Tukey's multiple-comparison test (Fig. 9B), as well as two-way ANOVA with Dunnett's multiple-comparison test (Fig. 8B), were performed using the GraphPad Prism 8 software.

ACKNOWLEDGMENTS

We thank Stephan Becker (Philipps University Marburg) for providing Huh7 cells and Friedemann Weber (Justus Liebig University Giessen) for providing the pI.18-HA-PKRdelE7 plasmid.

Funding was provided by the Deutsche Forschungsgemeinschaft (DFG; grant 389002253 [L.W. and J.B.]), as well as intramural funding from the Friedrich-Loeffler-Institut (D.S.U., A.G., and T.H.), including as part of the VISION consortium (M.J.P. and B.S.B.). The funders had no role in study design, data collection and interpretation, or the decision to submit the work for publication.

REFERENCES

1. Jacob ST, Crozier I, Fischer WA, II, Hewlett A, Kraft CS, Vega MA, Soka MJ, Wahl V, Griffiths A, Bollinger L, Kuhn JH. 2020. Ebola virus disease. Nat Rev Dis Primers 6:13. https://doi.org/10.1038/s41572-020-0147-3.
2. Markham A. 2021. REGN-EB3: first approval. Drugs 81:175–178. https://doi.org/10.1007/s40265-020-01452-3.
3. FDA. 2020. FDA approves treatment for Ebola virus. US Food and Drug Administration, Bethesda, MD. https://www.fda.gov/drugs/drug-safety-and-availability/fda-approves-treatment-ebola-virus.
4. Hoenen T, Jung S, Herwig A, Groseth A, Becker S. 2010. Both matrix proteins of Ebola virus contribute to the regulation of viral genome replication and transcription. Virology 403:56–66. https://doi.org/10.1016/j.virol.2010.04.002.
5. Mühlberger E, Weik M, Volchkov VE, Klenk HD, Becker S. 1999. Comparison of the transcription and replication strategies of Marburg virus and Ebola virus by using artificial replication systems. J Virol 73:2333–2342. https://doi.org/10.1128/JVI.73.3.2333-2342.1999.
6. Kruse T, Biedenkopf N, Hertz EPT, Dietzel E, Stalmann G, Lopez-Mendez B, Davey NE, Nilsson J, Becker S. 2018. The Ebola virus nucleoprotein recruits the host PP2A-B56 phosphatase to activate transcriptional support activity of VP30. Mol Cell 69:136–145.e6. https://doi.org/10.1016/j.molcel.2017.11.034.
7. Takamatsu Y, Krahling V, Kolesnikova L, Halwe S, Lier C, Baumeister S, Noda T, Biedenkopf N, Becker S. 2020. Serine-arginine protein kinase 1 regulates Ebola virus transcription. mBio 11:e02565-19. https://doi.org/10.1128/mBio.02565-19.
8. Ilinykh PA, Tigabu B, Ivanov A, Ammosova T, Obukhov Y, Garron T, Kumari N, Kovalskyy D, Platonov MO, Naumchik VS, Freiberg AN, Nekhai S, Bukreyev A. 2014. Role of protein phosphatase 1 in dephosphorylation of Ebola virus VP30 protein and its targeting for the inhibition of viral transcription. J Biol Chem 289:22723–22738. https://doi.org/10.1074/jbc.M114.575050.
9. Batra J, Hultquist JF, Liu D, Shtanko O, Von Dollen J, Satkamp L, Jang GM, Luthra P, Schwarz TM, Small GI, Arnett E, Anantpadma M, Reyes A, Leung DW, Kaake R, Haas P, Schmidt CB, Schlesinger LS, LaCount DJ, Davey RA, Amarasinghe GK, Basler CF, Krogan NJ. 2018. Protein interaction mapping identifies RBBP6 as a negative regulator of Ebola virus replication. Cell 175:1917–1930. https://doi.org/10.1016/j.cell.2018.08.044.
10. Batra J, Mori H, Small GI, Anantpadma M, Shtanko O, Mishra N, Zhang M, Liu D, Williams CG, Biedenkopf N, Becker S, Gross ML, Leung DW, Davey RA, Amarasinghe GK, Krogan NJ, Basler CF. 2021. Non-canonical proline-tyrosine interactions with multiple host proteins regulate Ebola virus infection. EMBO J 40:e105568. https://doi.org/10.15252/embj.2020105658.
11. Chen J, He Z, Yuan Y, Huang F, Luo B, Zhang J, Pan T, Zhang H, Zhang J. 2019. Host factor SMYD3 is recruited by Ebola virus nucleoprotein to facilitate viral mRNA transcription. Emerg Microbes Infect 8:1347–1360. https://doi.org/10.1080/22221751.2019.1662736.
12. Hoenen T, Shabman RS, Groseth A, Herwig A, Weber M, Schudt G, Dolnik O, Basler CF, Becker S, Feldmann H. 2012. Inclusion bodies are a site of ebolavirus replication. J Virol 86:11779–11788. https://doi.org/10.1128/JVI.01525-12.
13. Lier C, Becker S, Biedenkopf N. 2017. Dynamic phosphorylation of Ebola virus VP30 in NP-induced inclusion bodies. Virology 512:39–47. https://doi.org/10.1016/j.virol.2017.09.006.
14. Groseth A, Charton JE, Sauerborn M, Feldmann F, Jones SM, Hoenen T, Feldmann H. 2009. The Ebola virus ribonucleoprotein complex: a novel VP30-L interaction identified. Virus Res 140:8–14. https://doi.org/10.1016/j.virusres.2008.10.017.
15. Miyake T, Farley CM, Neubauer BE, Beddow TP, Hoenen T, Engel DA. 2020. Ebola virus inclusion body formation and RNA synthesis are controlled by a novel domain of nucleoprotein interacting with VP35. J Virol 94:e02100-19. https://doi.org/10.1128/JVI.02100-19.
16. Becker S, Rinne C, Hofsass U, Klenk HD, Mühlberger E. 1998. Interactions of Marburg virus nucleocapsid proteins. Virology 249:406–417. https://doi.org/10.1006/viro.1998.9328.
17. Nikolic J, Le Bars R, Lama Z, Scrima N, Lagaudriere-Gesbert C, Gaudin Y, Blondel D. 2017. Negri bodies are viral factories with properties of liquid organelles. Nat Commun 8:58. https://doi.org/10.1038/s41467-017-00102-9.
18. Zhou Y, Su JM, Samuel CE, Ma D. 2019. Measles virus forms inclusion bodies with properties of liquid organelles. J Virol 93:e00948-19. https://doi.org/10.1128/JVI.00948-19.
19. Gomes E, Shorter J. 2019. The molecular language of membraneless organelles. J Biol Chem 294:7115–7127. https://doi.org/10.1074/jbc.TM118.001192.
20. Wendt L, Brandt J, Bodmer BS, Reiche S, Schmidt ML, Traeger S, Hoenen T. 2020. The Ebola virus nucleoprotein recruits the nuclear RNA export factor NXF1 into inclusion bodies to facilitate viral protein expression. Cells 9:187. https://doi.org/10.3390/cells9010187.
21. Heath CG, Viphakone N, Wilson SA. 2016. The role of TREX in gene expression and disease. Biochem J 473:2911–2935. https://doi.org/10.1042/BCJ20160010.
22. Köhler A, Hurt E. 2007. Exporting RNA from the nucleus to the cytoplasm. Nat Rev Mol Cell Biol 8:761–773. https://doi.org/10.1038/nrm2255.
23. Viphakone N, Hautbergue GM, Walsh M, Chang CT, Holland A, Folco EG, Reed R, Wilson SA. 2012. TREX exposes the RNA-binding domain of Nxf1 to enable mRNA export. Nat Commun 3:1006. https://doi.org/10.1038/ncomms2005.
24. Chen IH, Sciabica KS, Sandri-Goldin RM. 2002. ICP27 interacts with the RNA export factor Aly/REF to direct herpes simplex virus type 1 intronless mRNAs to the TAP export pathway. J Virol 76:12877–12889. https://doi.org/10.1128/jvi.76.24.12877-12889.2002.
25. Satterly N, Tsai PL, van Deursen J, Nussenzveig DR, Wang Y, Faria PA, Levay A, Levy DE, Fontoura BM. 2007. Influenza virus targets the mRNA export machinery and the nuclear pore complex. Proc Natl Acad Sci U S A 104:1853–1858. https://doi.org/10.1073/pnas.0610977104.
26. Tunnicliffe RB, Tian X, Storer J, Sandri-Goldin RM, Golovanov AP. 2018. Overlapping motifs on the herpes viral proteins ICP27 and ORF57 mediate interactions with the mRNA export adaptors ALYREF and UIF. Sci Rep 8:15005. https://doi.org/10.1038/s41598-018-33379-x.
27. Jackson BR, Boyne JR, Noerenberg M, Taylor A, Hautbergue GM, Walsh MJ, Wheat R, Blackbourn DJ, Wilson SA, Whitehouse A. 2011. An interaction between KSHV ORF57 and UIF provides mRNA-adaptor redundancy in herpesvirus intronless mRNA export. PLoS Pathog 7:e1002138. https://doi.org/10.1371/journal.ppat.1002138.
28. Martin S, Chiramel AI, Schmidt ML, Chen YC, Whitt N, Watt A, Dunham EC, Shifflett K, Traeger S, Leske A, Buehler E, Martellaro C, Brandt J, Wendt L, Müller A, Peitsch S, Best SM, Stech J, Finke S, Römer-Oberdörfer A, Groseth A, Feldmann H, Hoenen T. 2018. A genome-wide siRNA screen identifies a druggable host pathway essential for the Ebola virus life cycle. Genome Med 10:58. https://doi.org/10.1186/s13073-018-0570-1.
29. Leung DW, Borek D, Luthra P, Binning JM, Anantpadma M, Liu G, Harvey IB, Su Z, Endlich-Frazier A, Pan J, Shabman RS, Chiu W, Davey RA, Otwinowski Z,

Basler CF, Amarasinghe GK. 2015. An intrinsically disordered peptide from Ebola virus VP35 controls viral RNA synthesis by modulating nucleoprotein-RNA interactions. Cell Rep 11:376–389. https://doi.org/10.1016/j.celrep.2015.03.034.
30. Noda T, Watanabe S, Sagara H, Kawaoka Y. 2007. Mapping of the VP40-binding regions of the nucleoprotein of Ebola virus. J Virol 81:3554–3562. https://doi.org/10.1128/JVI.02183-06.
31. Sugita Y, Matsunami H, Kawaoka Y, Noda T, Wolf M. 2018. Cryo-EM structure of the Ebola virus nucleoprotein-RNA complex at 3.6 Å resolution. Nature 563:137–140. https://doi.org/10.1038/s41586-018-0630-0.
32. Watanabe S, Noda T, Kawaoka Y. 2006. Functional mapping of the nucleoprotein of Ebola virus. J Virol 80:3743–3751. https://doi.org/10.1128/JVI.80.8.3743-3751.2006.
33. Bharat TA, Noda T, Riches JD, Kraehling V, Kolesnikova L, Becker S, Kawaoka Y, Briggs JA. 2012. Structural dissection of Ebola virus and its assembly determinants using cryo-electron tomography. Proc Natl Acad Sci U S A 109:4275–4280. https://doi.org/10.1073/pnas.1120453109.
34. Noda T, Hagiwara K, Sagara H, Kawaoka Y. 2010. Characterization of the Ebola virus nucleoprotein-RNA complex. J Gen Virol 91:1478–1483. https://doi.org/10.1099/vir.0.019794-0.
35. Negredo A, Palacios G, Vazquez-Moron S, Gonzalez F, Dopazo H, Molero F, Juste J, Quetglas J, Savji N, de la Cruz Martinez M, Herrera JE, Pizarro M, Hutchison SK, Echevarria JE, Lipkin WI, Tenorio A. 2011. Discovery of an ebolavirus-like filovirus in europe. PLoS Pathog 7:e1002304. https://doi.org/10.1371/journal.ppat.1002304.
36. Baird NL, York J, Nunberg JH. 2012. Arenavirus infection induces discrete cytosolic structures for RNA replication. J Virol 86:11301–11310. https://doi.org/10.1128/JVI.01635-12.
37. Katahira J, Strasser K, Podtelejnikov A, Mann M, Jung JU, Hurt E. 1999. The Mex67p-mediated nuclear mRNA export pathway is conserved from yeast to human. EMBO J 18:2593–2609. https://doi.org/10.1093/emboj/18.9.2593.
38. Grüter P, Tabernero C, von Kobbe C, Schmitt C, Saavedra C, Bachi A, Wilm M, Felber BK, Izaurralde E. 1998. TAP, the human homolog of Mex67p, mediates CTE-dependent RNA export from the nucleus. Mol Cell 1:649–659. https://doi.org/10.1016/S1097-2765(00)80065-9.
39. Hautbergue GM, Hung ML, Golovanov AP, Lian LY, Wilson SA. 2008. Mutually exclusive interactions drive handover of mRNA from export adaptors to TAP. Proc Natl Acad Sci U S A 105:5154–5159. https://doi.org/10.1073/pnas.0709167105.
40. Hung ML, Hautbergue GM, Snijders AP, Dickman MJ, Wilson SA. 2010. Arginine methylation of REF/ALY promotes efficient handover of mRNA to TAP/NXF1. Nucleic Acids Res 38:3351–3361. https://doi.org/10.1093/nar/gkq033.
41. Luo ML, Zhou Z, Magni K, Christoforides C, Rappsilber J, Mann M, Reed R. 2001. Pre-mRNA splicing and mRNA export linked by direct interactions between UAP56 and Aly. Nature 413:644–647. https://doi.org/10.1038/35098106.
42. Strässer K, Masuda S, Mason P, Pfannstiel J, Oppizzi M, Rodriguez-Navarro S, Rondon AG, Aguilera A, Struhl K, Reed R, Hurt E. 2002. TREX is a conserved complex coupling transcription with messenger RNA export. Nature 417:304–308. https://doi.org/10.1038/nature746.
43. Bachi A, Braun IC, Rodrigues JP, Pante N, Ribbeck K, von Kobbe C, Kutay U, Wilm M, Gorlich D, Carmo-Fonseca M, Izaurralde E. 2000. The C-terminal domain of TAP interacts with the nuclear pore complex and promotes export of specific CTE-bearing RNA substrates. RNA 6:136–158. https://doi.org/10.1017/s1355838200991994.
44. Fribourg S, Braun IC, Izaurralde E, Conti E. 2001. Structural basis for the recognition of a nucleoporin FG repeat by the NTF2-like domain of the TAP/p15 mRNA nuclear export factor. Mol Cell 8:645–656. https://doi.org/10.1016/s1097-2765(01)00348-3.
45. Hirai Y, Tomonaga K, Horie M. 2021. Borna disease virus phosphoprotein triggers the organization of viral inclusion bodies by liquid-liquid phase separation. Int J Biol Macromol 192:55–63. https://doi.org/10.1016/j.ijbiomac.2021.09.153.
46. Geisbert TW, Jahrling PB. 1995. Differentiation of filoviruses by electron microscopy. Virus Res 39:129–150. https://doi.org/10.1016/0168-1702(95)00080-1.
47. Garcia-Serradilla M, Risco C. 2021. Light and electron microscopy imaging unveils new aspects of the antiviral capacity of silver nanoparticles in bunyavirus-infected cells. Virus Res 302:198444. https://doi.org/10.1016/j.virusres.2021.198444.
48. Barr JN. 2007. Bunyavirus mRNA synthesis is coupled to translation to prevent premature transcription termination. RNA 13:731–736. https://doi.org/10.1261/rna.436607.
49. Brandt J, Wendt L, Bodmer BS, Mettenleiter TC, Hoenen T. 2020. The cellular protein CAD is recruited into Ebola virus inclusion bodies by the nucleoprotein NP to facilitate genome replication and transcription. Cells 9:1126. https://doi.org/10.3390/cells9051126.
50. Bodmer BS, Zierke L, Wendt L, Gressler J, Groseth A, Hoenen T. 2021. Remdesivir inhibits the polymerases of the novel filoviruses Lloviu and Bombali virus. Antiviral Res 192:105120. https://doi.org/10.1016/j.antiviral.2021.105120.
51. Dunham EC, Leske A, Shifflett K, Watt A, Feldmann H, Hoenen T, Groseth A. 2018. Lifecycle modelling systems support inosine monophosphate dehydrogenase (IMPDH) as a pro-viral factor and antiviral target for New World arenaviruses. Antiviral Res 157:140–150. https://doi.org/10.1016/j.antiviral.2018.07.009.
52. Kämper L, Zierke L, Schmidt ML, Müller A, Wendt L, Brandt J, Hartmann E, Braun S, Holzerland J, Groseth A, Hoenen T. 2019. Assessment of the function and intergenus-compatibility of Ebola and Lloviu virus proteins. J Gen Virol 100:760–772. https://doi.org/10.1099/jgv.0.001261.
53. Pickin MJ, Devignot S, Weber F, Groschup MH. 2022. Comparison of Crimean-Congo hemorrhagic fever virus and Aigai virus in life cycle modeling systems reveals a difference in l protein activity. J Virol 96:e0059922. https://doi.org/10.1128/jvi.00599-22.
54. Klemm C, Reguera J, Cusack S, Zielecki F, Kochs G, Weber F. 2013. Systems to establish bunyavirus genome replication in the absence of transcription. J Virol 87:8205–8212. https://doi.org/10.1128/JVI.00371-13.